
π -StepNFT: Wider Space Needs Finer Steps in Online RL for Flow-based VLAs

Siting Wang^{1,2,3} Xiaofeng Wang^{1,4} Zheng Zhu^{1,†} Minnan Pei^{2,3} Xinyu Cui^{2,3,5}
 Cheng Deng⁶ Jian Zhao⁵ Guan Huang¹ Haifeng Zhang^{2,3} Jun Wang^{7,†}

Abstract

Flow-based vision-language-action (VLA) models excel in embodied control but suffer from intractable likelihoods during multi-step sampling, hindering online reinforcement learning. We propose π -StepNFT (Step-wise Negative-aware Fine-Tuning), a critic-and-likelihood-free framework that requires only a single forward pass per optimization step and eliminates auxiliary value networks. We identify that wider exploration spaces necessitate finer-grained, step-wise guidance for alignment. Empirically, π -StepNFT unlocks latent potential on LIBERO with competitive few-shot robustness. Moreover, it achieves superior generalization on ManiSkill, outperforming value-based baselines in OOD scenarios by preventing overfitting to multimodal features. This property offers a scalable solution promising for complex real-world applications. Our implementation builds upon RLinf and is publicly available at <https://wangst0181.github.io/pi-StepNFT/>.

1. Introduction

Vision-language-action (VLA) models have recently demonstrated increasingly general capabilities, enabling robots to follow open-ended natural language instructions and perform complex tasks across diverse environments. While early approaches discretized actions into tokens (Zitkovich et al., 2023; Kim et al., 2024) or mapped observations to continuous regression features (Kim et al., 2025b), recent advances have converged on flow-matching-based policies (Black et al., 2026; 2025; Intelligence et al., 2025; Ye et al., 2025; Bjorck et al., 2025). These models, by integrating large-scale vision-language pretraining with generative action prediction, have established a new standard for complex manipulation tasks.

¹GigaAI ²Institute of Automation, Chinese Academy of Sciences ³University of Chinese Academy of Sciences ⁴Tsinghua University ⁵Zhongguncun Academy ⁶The University of Edinburgh ⁷University College London. Correspondence to: Zheng Zhu <zhengzhu@iee.org>.

A recent systematic analysis (Pan et al., 2025) suggests that after supervised fine-tuning (SFT) converges, the output of flow-based VLAs often collapses to a single mode. Consequently, their efficacy stems from a mechanism of *stochasticity injection* combined with *supervised iterative correction*. Injecting noise during training and iterative correction during inference enable the policy to resist error accumulation and adhere closely to the expert manifold during closed-loop execution. However, we contend that relying heavily on the density of expert demonstrations, SFT merely establishes a foundational behavioral manifold that resembles a *narrow line*, where the model often lacks the ability to recover once it deviates due to micro-perturbations during testing. To overcome this fragility, reinforcement learning (RL) is required, aiming not to learn from scratch, but to *explore an expanded manifold* around the expert trajectory, endowing the model with the local error-correction capabilities needed to mitigate state deviations.

However, training flow-based VLAs with RL faces fundamental bottlenecks. The deterministic nature of ordinary differential equation (ODE) trajectories confines the action exploration space entirely to the initial noise distribution. To this end, the multi-step ODE integration renders exact action likelihoods computationally intractable, as calculating gradients requires expensive Jacobian trace estimation or backpropagation through the solver. Faced with these challenges, existing solutions either bypass likelihoods by employing latent space value distillation (Li et al., 2025b) or training separate value functions to introduce explicit conditioning on trajectory quality (Intelligence et al., 2025), or approximate likelihoods via Gaussian parameterization at each denoising step (Chen et al., 2025). In contrast, Diffusion-NFT (Zheng et al., 2026) offers a likelihood-free alternative from the image generation domain. It optimizes the flow field directly on the forward diffusion process and defines a contrastive improvement direction by splitting samples into positive and negative subsets.

Crucially, directly transferring Diffusion-NFT to embodied control reveals a fundamental domain gap. While the standard deterministic ODE sampling yields a safe but narrow manifold, it lacks the exploratory capacity for self-improvement. Attempting to broaden this scope via stochastic differential equation (SDE) theoretically enables mani-

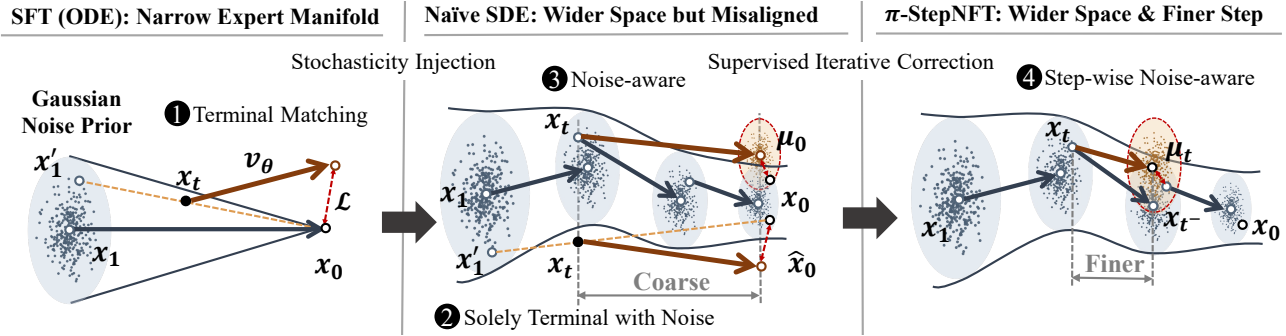


Figure 1. Comparison of training paradigms. **Left (ODE):** Terminal supervision is well-posed for deterministic ODEs but results in a narrow expert manifold. **Middle (Naïve SDE):** Stochastic rollouts introduce a wider exploration space, but coarse terminal supervision fails to correct deviations, leading to misalignment. **Right (π -StepNFT):** Our method leverages the wider space from SDE but applies finer, step-wise ranking guidance to ensure robust alignment with the expert manifold.

fold expansion during exploration, yet in practice, it results in a wider space but misaligned policy. This failure stems from the nature of supervision. Unlike image generation that targets static distribution matching, embodied control is sequential and thus sensitive to compounding errors. Moreover, embodied control typically uses a short denoising path to meet interaction latency, and prior empirical evidence indicates diminishing returns from moderately longer paths (Chen et al., 2025), making fine-grained, step-wise denoising supervision feasible in practice.

As illustrated in Figure 1, under deterministic ODE rollouts, the intermediate state x_t stays on a narrow trajectory, making “point-level” terminal matching 1 on x_0 relatively well-posed. However, under SDE rollouts, injected noises accumulate along the denoising path, and naively regressing the final x_0 forces unstable point-to-point matching with high-variance gradients. A noise-aware view 2 reveals that each denoising update induces a Gaussian transition, suggesting “region-level” supervision with variance-normalization; yet using only the solely terminal 3 still yields a coarse correction that lags behind on-policy drift. This motivates step-wise supervision 4 that targets the immediate next solver state x_{t-} , providing fine-grained local guidance to stabilize stochastic exploration and accelerate convergence.

To address these issues, we propose π -StepNFT, a critic-and-likelihood-free online RL framework tailored for embodied VLAs. We achieve robust manifold expansion by systematically redesigning the interplay between *exploration* and *supervision*. First, regarding *lack of exploration*, effective policy improvement necessitates a wider behavioral space. We introduce an SDE-based sampling mechanism during training that augments deterministic rollouts with structured noise, forcing the model to traverse adjacent states to effectively inflate the behavioral manifold. Second, for *supervision target mismatch*, anchoring this expanded exploration demands finer-grained step-wise supervision. We shift the prediction target from the final denoised out-

put x_0 to the immediate next denoising step x_{t-} , using a noise-based regression to generate the precise local gradients needed for robust alignment. Third, regarding *suppressed successful exploration*, we identify that the previous objective in Diffusion-NFT suffers from an “implicit penalty”, which inadvertently suppresses policy updates to minimize the magnitude of branch separation. To overcome this, we introduce a logistic contrastive ranking loss, establishing a “push-pull dynamics”: maximizing the likelihood of successful trajectories while suppressing failed ones. This noise-based, step-wise, bidirectional and penalty-free signal enforces strict preference separation, enabling more aggressive and precise policy improvement.

In summary, our main contributions are as follows:

- We propose π -StepNFT, a critic-and-likelihood-free online RL framework tailored for flow-based VLAs, which eliminates the need to train auxiliary value networks that are prone to multimodal overfitting, and requires only a single forward pass per optimization step.
- We identify that wider exploration spaces induced by SDE necessitate finer-grained guidance. By shifting the supervision target from the terminal to the immediate next denoising step and incorporating a logistic contrastive ranking objective, we resolve the supervision mismatch and reinforce successful exploration.
- We validate our approach through extensive experiments on LIBERO (Liu et al., 2023) and ManiSkill (Mu et al., 2021) benchmarks. On LIBERO, π -StepNFT unlocks the policy’s potential in few-shot settings, achieving a **32.9% improvement** over SFT. On ManiSkill, it demonstrates superior generalization in visually diverse OOD settings by preventing critic-induced multimodal overfitting, outperforming critic-based baselines by **11.1%** in unseen scenarios, highlighting its potential for complex real-world deployment.

2. Related Works

2.1. Online RL for VLAs

Recent VLA models have evolved from discrete tokenization (Zitkovich et al., 2023; Kim et al., 2024; Liu et al., 2026) to continuous flow-based policies (Ghosh et al., 2024; Black et al., 2026; 2025; Intelligence et al., 2025), which establish strong priors for manipulation. However, fine-tuning these flow-based VLAs faces the challenge of intractable action likelihoods due to multi-step ODE sampling. Existing solutions generally adopt two strategies to circumvent this: bypassing likelihood calculation via value distillation or preference feedback (e.g., GR-RL (Li et al., 2025b), $\pi_{0.6}^*$), or approximating likelihoods by transforming ODEs into SDEs (e.g., π_{RL} (Chen et al., 2025)). Similar to test-time scaling strategies (Yang et al., 2025; Song et al., 2025), noise injection in SDEs facilitates exploration, yet existing methods often struggle to balance exploration width with supervision granularity.

2.2. Policy Optimization for Generative Models

To handle intractable likelihoods in generative policy optimization, prior works typically follow three paradigms. Explicit gradient and advantage methods (Black et al., 2023; Liu et al., 2025; Zhang et al., 2025b) treat denoising as a sequential process but often require expensive backpropagation through solvers. Reward-Weighted methods (Pfrommer et al., 2025; Fan et al., 2025; McAllister et al., 2025) avoid exact likelihoods by re-weighting regression targets, yet they can suffer from high variance in gradient estimation. Preference and contrastive methods (Wallace et al., 2024; Zhang et al., 2025a) offer a more stable alternative by aligning distributions via ranking. Most notably, Diffusion-NFT (Zheng et al., 2026) proposes a likelihood-free framework using implicit forward-process updates. Our work extends this efficient paradigm to embodied control, addressing the unique supervision gaps that arise when applying it to multi-step VLA policies. Please refer to Appendix B for detailed related works.

3. Preliminaries

We use two time scales throughout the paper: environment steps and denoising time. An episode trajectory is indexed by environment steps $i = 0, \dots, H - 1$, yielding $\tau = \{(s_i, a_i)\}_{i=0}^{H-1}$. Separately, the flow policy uses a continuous denoising time $t \in [0, 1]$ (or a discretization) to generate an action. When discretized, we use K solver steps with schedule $1 = t_0 > t_1 > \dots > t_K = 0$, and denote intermediate sampler states by $\{x_{t_j}\}_{j=0}^K$, where K is typically small in embodied control due to real-time constraints. Unless stated otherwise, t refers to denoising time in the sampler, while the environment index is i , avoiding ambi-

guity when both the RL objective and the flow dynamics appear in the same derivations.

3.1. Flow Matching for VLA Models

We consider a VLA policy that generates continuous actions $x_0 \in \mathbb{R}^d$ conditioned on context c . Flow-matching (Lipman et al., 2022) learns a time-dependent vector field $v_\theta(x, t, c)$ to generate data by transforming a noise distribution $x_1 \sim \mathcal{N}(0, I)$ to the data distribution x_0 over time $t \in [0, 1]$.

The standard flow-matching objective regresses the network prediction v_θ onto the target field $u_t = x_1 - x_0$ by minimizing $\mathcal{L}_{CFM}(\theta) = \mathbb{E}_{t, x_0, x_1} [\|v_\theta(x_t, t, c) - u_t\|^2]$, where $x_t = tx_1 + (1 - t)x_0$.

ODE Sampling. In the standard deterministic setting, inference is performed by numerically integrating the ODE $dx = v_\theta(x, t, c)dt$ from $t = 1$ to $t = 0$. Using a discrete step size $\delta_t > 0$, the Euler update rule for the next step x_{t^-} (where $t^- = t - \delta_t$) is:

$$x_{t^-} = x_t - v_\theta(x_t, t, c)\delta_t. \quad (1)$$

While efficient for generation, this deterministic trajectory lacks the exploratory capability required for reinforcement learning.

SDE Sampling. To enable exploration, we adopt the reverse-time SDE formulation (Liu et al., 2025), which injects stochasticity while preserving the marginal distribution. The Euler-Maruyama discretized update is given by:

$$x_{t^-} = x_t + \left[v_\theta(x_t, t) + \frac{\sigma_t^2}{2t}(x_t + (1 - t)v_\theta(x_t, t)) \right] (-\delta_t) + \sigma_t \sqrt{\delta_t} \epsilon, \quad (2)$$

where $\epsilon \sim \mathcal{N}(0, I)$ provides exploration noise. This update step induces a Gaussian transition density $q_{\theta, t}(x_{t^-} | x_t, c) = \mathcal{N}(\mu_{\theta, t}(x_t), \Sigma_t)$. Crucially, the mean of this transition is an affine transformation of the network output:

$$\mu_{\theta, t}(x_t, c) = U_t(x_t, t) + B_t(t)v_\theta(x_t, t, c), \quad (3)$$

where U_t and B_t are pre-determined coefficients derived from the noise schedule (detailed in Appendix A.1).

This linear relationship allows us to propagate gradients efficiently from the transition target to the policy parameters without backpropagating through the ODE solver.

3.2. RL Fine-tuning and the Likelihood Gap

We formulate the fine-tuning task as maximizing the expected return $J(\theta)$ over trajectories $\tau = (s_0, a_0, \dots)$: $J(\theta) = \mathbb{E}_{\tau \sim p_\theta(\tau)} [R(\tau)]$, where the trajectory distribution is determined by the environment dynamics and the policy: $p_\theta(\tau) = p(s_0) \prod_{i=0}^{H-1} \pi_\theta(a_i | s_i) p(s_{i+1} | s_i, a_i)$.

Algorithm 1 π -StepNFT: Step-wise Negative-aware Fine-Tuning with Contrastive Ranking

Require: Flow policy $\pi_{\theta^{\text{old}}}$, simulator \mathcal{E} , env steps H , solver steps K , schedule $\{t_j\}_{j=0}^K$, hyperparams $\beta, \lambda_{\text{TR}}$. Initialize $\theta \leftarrow \theta^{\text{old}}$, buffer $\mathcal{D} \leftarrow \emptyset$.

for each iteration m **do**
 // Phase 1: Data Collection
for each task (initial state s_0 , language prompt c) **do**
 Rollout H env steps using $\pi_{\theta^{\text{old}}}$.
for $i = 0$ **to** $H - 1$ **do**
 Run Flow-SDE sampler; get chain $\{x_{t_j}\}_{j=0}^K$.
 Sample $j \sim \mathcal{U}\{0, \dots, K - 1\}$; set $t \leftarrow t_j$.
 Set $x_t \leftarrow x_{t_j}$ and $x_{t^-} \leftarrow x_{t_{j+1}}$.
 Set $v_t^{\text{old}} \leftarrow \pi_{\theta^{\text{old}}}(c, s_i, x_t, t)$.
 Record $d_i = (x_t, x_{t^-}, v_t^{\text{old}}, t, s_i, c)$.
 Execute x_{t_K} in \mathcal{E} and update s_i
end for
 Observe terminal $r \in \{0, 1\}$; $\mathcal{D} \leftarrow \{(d_i, r)\}_{i=0}^{H-1}$.
end for
 // Phase 2: Optimization
for each batch $(x_t, x_{t^-}, v_t^{\text{old}}, t, s, c, r) \sim \mathcal{D}$ **do**
 Pred $v_{\theta, t} \leftarrow \pi_{\theta}(c, s, x_t, t)$; Drift $\Delta v_{\theta} \leftarrow v_{\theta, t} - v_t^{\text{old}}$.
 Construct mirrors: $v_{\theta}^{\pm} \leftarrow v_t^{\text{old}} \pm \beta \Delta v_{\theta}$.
 Calc means/var: $\mu_{\theta, t}^{\pm}, \Sigma_t \leftarrow \text{Mean_Var}(x_t, v_{\theta}^{\pm}, t)$.
 Calc errors: $E_{\theta, t}^{\pm} \leftarrow \|x_{t^-} - \mu_{\theta, t}^{\pm}\|_{\Sigma_t^{-1}}^2$.
 Set $y \leftarrow 2r - 1$ and $\Delta E_{\theta} \leftarrow E_{\theta, t}^+ - E_{\theta, t}^-$.
 $\mathcal{L}_{\text{total}} \leftarrow \text{softplus}(\frac{1}{2}y\Delta E_{\theta}) + \lambda_{\text{TR}}\|\Delta v_{\theta}\|^2$.
 Update $\theta \leftarrow \theta - \eta \nabla_{\theta} \mathcal{L}_{\text{total}}$.
end for
 $\theta^{\text{old}} \leftarrow \alpha_m \theta^{\text{old}} + (1 - \alpha_m)\theta$; clear \mathcal{D} .
end for
Output: Optimized policy π_{θ} .

Standard policy gradient methods rely on the score function: $\nabla_{\theta} J(\theta) = \mathbb{E}_{\tau} [\sum_i \nabla_{\theta} \log \pi_{\theta}(a_i | s_i) \cdot \Psi_i]$, where Ψ_i is the advantage or return (e.g., REINFORCE (Williams, 1992), PPO (Schulman et al., 2017)).

However, for flow-based policies, calculating the explicit log-likelihood $\log \pi_{\theta}(a_i | s_i)$ is computationally expensive and numerically unstable, as it requires integrating the instantaneous change of variables (Jacobian trace) along the entire generation trajectory. This intractability prevents the direct application of standard RL algorithms, motivating our likelihood-free approach.

4. Method

We introduce π -StepNFT (Step-wise Negative-aware Fine-Tuning), an online RL framework designed for flow-based VLA models, as shown in Algorithm 1. Our method is inspired by Diffusion-NFT (Zheng et al., 2026), which fine-tunes diffusion models using a weighted-MSE objective on the final denoised output x_0 generated by ODE rollouts.

Wider Space Needs Finer Steps. While effective for image generation, we observe that directly transferring the ODE-based formulation to embodied control yields suboptimal convergence. We attribute this domain gap to two critical factors, requiring us to establish a *Wider Space* for exploration anchored by *Finer Steps* of supervision (made practical by the typically short denoising path in embodied control):

- **Lack of Exploration:** Deterministic ODE rollouts quickly collapse to a narrow manifold, failing to discover diverse solutions in high-dimensional action spaces. We instead adopt an SDE-based formulation to inject controlled noise. This active expansion creates the necessary *wider space* for the policy to traverse and learn from adjacent regions around the expert trajectory.
- **Supervision Target Mismatch:** Operating within this wider space renders standard terminal- x_0 supervision unstable, as injected noises accumulate and amplify variance over the rollout horizon. To counteract this, we require *finer steps* of guidance: we supervise the immediate one-step transition $x_t \rightarrow x_{t^-}$ with variance normalization, providing the precise, low-variance local gradients needed for robust alignment.

4.1. Step-wise Transitions and Mirror Errors

We conduct rollouts using the Flow-SDE solver described in Section 3.1 with a rollout policy $\pi_{\theta^{\text{old}}}$ which is updated with EMA across iterations. Each episode yields an environment trajectory $\tau = \{(s_i, a_i)\}_{i=0}^{H-1}$. At each environment step i , the policy generates a_i by running a K -step solver with schedule $1 = t_0 > t_1 > \dots > t_K = 0$, producing sampler states $\{x_{t_j}^{(i)}\}_{j=0}^K$; we execute the chunked terminal sample $x^{(i)} t_K$ in the simulator as a_i . For efficiency, we uniformly sample one solver index $j \sim \mathcal{U}\{0, \dots, K - 1\}$ and define a single solver transition $(x_t, x_{t^-}, t) = (x_{t_j}^{(i)}, x_{t_{j+1}}^{(i)}, t_j)$, where t^- denotes the next solver time point in the discretization. We additionally record the rollout velocity $v^{\text{old}} = \pi_{\theta^{\text{old}}}(c, x_t, t)$. Each episode also provides a terminal optimality signal $r(\tau) \in [0, 1]$.

Following Diffusion-NFT, we construct two “mirrored” velocity candidates $v^+ \theta$ and $v^- \theta$, symmetric around v^{old} along the update direction $\Delta v_{\theta} = v_{\theta} - v^{\text{old}}$:

$$v_{\theta}^+ = (1 - \beta)v^{\text{old}} + \beta v_{\theta}, \quad (4)$$

$$v_{\theta}^- = (1 + \beta)v^{\text{old}} - \beta v_{\theta}, \quad (5)$$

where $\beta > 0$ is a trust-region hyperparameter controlling how far we deviate from the rollout policy to estimate a local improvement signal. This construction ensures symmetry: $v_{\theta}^+ - v^{\text{old}} = v^{\text{old}} - v_{\theta}^- = \beta \Delta v_{\theta}$.

Importantly, under the Flow-SDE transition Eq. (3), the one-step mean is an affine function of the velocity, so these two velocity candidates induce two Gaussian transition means $\mu^\pm\theta, t = \mu_t(v^\pm\theta)$ with shared covariance Σ_t . We then compute the variance-normalized step errors against the sampled next state x_{t-} :

$$E_{\theta,t}^+ = \|x_{t-} - \mu_{\theta,t}^+\|_{\Sigma_t^{-1}}^2, \quad E_{\theta,t}^- = \|x_{t-} - \mu_{\theta,t}^-\|_{\Sigma_t^{-1}}^2. \quad (6)$$

Intuitively, $E_{\theta,t}^+$ measures how well the positive mirrored branch explains the observed stochastic transition, while $E_{\theta,t}^-$ measures the negative branch. Normalizing by Σ_t (which reflects the injected noise level at solver time t) stabilizes gradient scales across timesteps. We next show how this yields a step-wise contrastive objective over mirrored perturbations.

4.2. π -StepNFT: Step-wise Contrastive Objective

Given a sampled solver transition ($x_t \rightarrow x_{t-}$) with terminal signal $r(\tau)$, we define $y = 2r(\tau) - 1$. We use *oracle* to denote the ideal, outcome-conditioned comparison between $p(x_{t-} \mid x_t, c, o=1)$ and $p(x_{t-} \mid x_t, c, o=0)$, which is not directly observable. Our method replaces this with a computable ranking surrogate: we construct two *symmetric perturbations* around the rollout policy along the update direction and rank the two branches by which one assigns higher likelihood to the observed transition.

Definition 4.1 (π -StepNFT Objective). For a sampled solver transition tuple (x_t, x_{t-}, t, c) with episode label $y \in [-1, 1]$, let $E_{\theta,t}^+$ and $E_{\theta,t}^-$ denote the step-wise errors defined in Section 4.1. The step-level objective is:

$$\ell_t(\theta) = \text{softplus}\left(\frac{1}{2}y \cdot (E_{\theta,t}^+ - E_{\theta,t}^-)\right). \quad (7)$$

Minimizing ℓ_t encourages $E_{\theta,t}^+ < E_{\theta,t}^-$ when the episode is successful ($y > 0$) and reverses the inequality for failures ($y < 0$). Intuitively, this ranks two local transition hypotheses along the update direction $\Delta v_\theta = v_\theta - v^{\text{old}}$, using the episode label as a weak preference signal.

Lemma 4.2 (Log-Likelihood Ratio). *Under the shared covariance Σ_t , the difference in squared errors is proportional to the log-likelihood ratio of the two mirrored branches:*

$$\log \frac{q_{\theta,t}^+(x_{t-} \mid x_t, c)}{q_{\theta,t}^-(x_{t-} \mid x_t, c)} = -\frac{1}{2}(E_{\theta,t}^+ - E_{\theta,t}^-). \quad (8)$$

Proof. See Appendix A.2.

Lemma 4.2 shows that minimizing $\ell_t(\theta)$ adjusts the constructed transition log-ratio $\log\left(\frac{q_\theta^+}{q_\theta^-}\right)$ according to the episode label y . The two densities q_θ^\pm arise from symmetric perturbations $\pm\beta\Delta v_\theta$ of the rollout policy, so this

log-ratio provides a directional signal on the same observed solver transition ($x_t \rightarrow x_{t-}$). In contrast, DPO (Rafailov et al., 2023) ranks *outcome-conditioned* distributions under a shared context, whereas we rank *update perturbations* using only episode-level feedback. For $y = +1$, minimizing the loss increases the log-ratio, favoring updates that make the observed transition more likely under the positive perturbation; for $y = -1$, it encourages the opposite preference. Thus, ℓ_t yields a low-variance step-wise surrogate, and in Section 4.3 we show that under small-step assumptions its induced updates align with the oracle improvement direction from outcome-conditioned posterior splits.

4.3. Validity and Optimized Direction

This section closes the conceptual loop between our constructed step-wise objective and the oracle improvement signal.

Oracle direction from posterior splits (not directly computable). Let $o \in 0, 1$ denote the latent episode outcome under context c . Posterior splits (Appendix A.4) induce an outcome-conditioned decomposition of the rollout posterior at solver time t , which defines the oracle mean gap $\Delta\mu_t^*(x_t, c)$ (Lemma A.4). Intuitively, $\Delta\mu_t^*$ captures how the one-step transition mean would change if we could condition the rollout transition on success versus failure; we treat it as an ideal local improvement direction in mean space. Importantly, this oracle quantity is a reference defined under outcome conditioning, and is not directly observable from online rollouts.

Proposition 4.3 (Bayes Monotonicity). *For fixed (x_t, c) , the posterior $\mathbb{P}(o = 1 \mid x_{t-}, x_t, c)$ is strictly increasing in the oracle likelihood ratio $\frac{p(x_{t-} \mid x_t, c, o=1)}{p(x_{t-} \mid x_t, c, o=0)}$.*

Proof. See Appendix A.3.

Proposition 4.3 provides the key monotonic link: increasing the oracle transition ratio on the observed transition ($x_t \rightarrow x_{t-}$) strictly increases the posterior probability of success. This motivates seeking a step-wise objective that increases a success-vs-failure transition ratio, while acknowledging that the oracle-conditioned densities $p(\cdot \mid o)$ are inaccessible.

Computable surrogate via mirrored transitions (what we actually optimize). Since the oracle success–failure ratio $\frac{p(o=1)}{p(o=0)}$ is not observable online, we optimize a constructed step-wise surrogate based on the mirrored perturbations defined in Section 4.1. By Lemma 4.2, our ranking loss is equivalent to increasing (for $y > 0$) or decreasing (for $y < 0$) the constructed transition ratio $\frac{q_\theta^+}{q_\theta^-}$ evaluated on the observed transition ($x_t \rightarrow x_{t-}$). We next show that, under a small-step regime, the expected gradient induced by this constructed ratio aligns with the oracle mean-gap direction.

Theorem 4.4 (Gradient Form and Small-Step Alignment).

Let $e_t = x_{t^-} - \mu_t^{\text{old}}$ be the residual of the rollout mean, $d_t = \mu_{\theta,t}^+ - \mu_t^{\text{old}}$ be the displacement in mean space and B_t be the affine coefficient from Eq. (3).

(a) The error difference satisfies

$$E_{\theta,t}^+ - E_{\theta,t}^- = -4\langle \Sigma_t^{-1} e_t, d_t \rangle. \quad (9)$$

(b) Consequently, the gradient of the step loss ℓ_t is

$$-\nabla_{\theta} \ell_t(\theta) \propto \sigma(z_t) y \left(\frac{\partial v_{\theta}}{\partial \theta} \right)^{\top} B_t \Sigma_t^{-1} e_t, \quad (10)$$

where z_t is the softplus logit and $\sigma(\cdot)$ is the sigmoid.

(c) In the binary-success setting and for small updates ($v_{\theta} \approx v^{\text{old}}$ so $\sigma(z_t) \approx \text{const}$), the conditional expected direction aligns with the oracle mean gap:

$$\mathbb{E}[-\nabla_{\theta} \ell_t(\theta) \mid x_t, c] \parallel \left(\frac{\partial v_{\theta}}{\partial \theta} \right)^{\top} B_t \Sigma_t^{-1} \Delta \mu_t^*(x_t, c), \quad (11)$$

where $\Delta \mu_t^*$ is defined by posterior splits in Appendix A.4.

Proof. See Appendix A.5.

Theorem 4.4 provides the missing ‘‘closed loop’’: posterior splits define an *oracle* local improvement signal $\Delta \mu_t^*$, while our mirrored construction yields a *computable* surrogate ratio whose small-step expected gradient provably points in the same mean-space direction.

4.4. Comparison with Diffusion-NFT (Weighted-MSE)

Diffusion-NFT optimizes a reward-weighted regression objective. In our step-wise setting, the analogous form is $\ell_t^{\text{wMSE}}(\theta) = r E_{\theta,t}^+ + (1-r) E_{\theta,t}^-$, where $E_{\theta,t}^{\pm}$ are the mirrored step errors from Section 4.1. We next show that this weighted-MSE contains an *implicit separation penalty* that can suppress branch separation (and hence policy updates), whereas our logistic ranking objective isolates the directional alignment signal and induces a clearer push-pull behavior.

Theorem 4.5 (Separation Penalty in wMSE). *The wMSE loss decomposes as:*

$$\ell_t^{\text{wMSE}}(\theta) = \text{const} - 2y \langle \Sigma_t^{-1} e_t, d_t \rangle + \|d_t\|_{\Sigma_t^{-1}}^2. \quad (12)$$

Proof. See Appendix A.6.

Here, defined in Section 4.3, $e_t = x_{t^-} - \mu_t^{\text{old}}$ is the rollout residual and $d_t = \mu_{\theta,t}^+ - \mu_t^{\text{old}}$ is the mirrored mean displacement. The middle term is the directional alignment signal driven by y , while the last term $\|d_t\|_{\Sigma_t^{-1}}^2$ is a separation penalty that discourages large branch displacement irrespective of y .

In contrast, the core directional term in π -StepNFT (derived in Theorem 4.4) depends only on the error difference:

$$E_{\theta,t}^+ - E_{\theta,t}^- = -4\langle \Sigma_t^{-1} e_t, d_t \rangle. \quad (13)$$

Implicit Penalty: The decomposition of the objective above shows that wMSE optimizes the same alignment term *plus* an additional quadratic penalty $\|d_t\|_{\Sigma_t^{-1}}^2$. This penalty explicitly discourages branch separation (and thus suppresses the magnitude of the policy update), even when the data suggests a strong corrective move (i.e., large alignment between e_t and d_t). In contrast, by using a logistic ranking loss, π -StepNFT removes this intrinsic suppression and preserves the alignment signal as the dominant driver for policy improvement.

Push-pull dynamics: In the binary case $r \in \{0, 1\}$, the wMSE objective reduces to fitting only one branch: it *pulls* the selected branch toward the observed transition but does not explicitly *push* the other branch away. By contrast, our logistic ranking enforces a strict ordering between $E_{\theta,t}^+$ and $E_{\theta,t}^-$: for successful episodes it simultaneously pulls the positive branch and pushes the negative branch away (and vice versa for failures). This bidirectional signal yields stronger separation and typically sharper gradients during fine-tuning, which translates into faster convergence and higher asymptotic performance in our experiments.

5. Experiments

5.1. Experimental Setup

Evaluation Benchmarks. We evaluate on 2 multitask benchmarks. For LIBERO (Liu et al., 2023), we follow the standard protocol across four suites (Spatial, Object, Goal, Long), reporting average success rates over 500 episodes (50 states \times 10 sub-tasks) per suite. For ManiSkill (Mu et al., 2021), we adopt the PutOnPlateInScene multitask setting from RL4VLA (Liu et al., 2026) tested for generalization, which defines 4,352 compositional tasks derived from 16 objects, 17 receptacles, and 16 tabletop scenes.

Model Architectures. We employ π_0 and $\pi_{0.5}$, OpenPi’s flow-based VLAs combining a PaliGemma-3B (Beyer et al., 2024; Steiner et al., 2024) backbone with a \sim 300M parameter flow-matching action expert. $\pi_{0.5}$ incorporates an improved training paradigm. Adhering to official configurations, π_0 uses vision, text, and proprioception, while $\pi_{0.5}$ omits proprioception on LIBERO; this modality setting remains consistent across SFT and RL phases.

SFT Initialization. We initialize our policy using π_{RL} checkpoints. For LIBERO, to prevent performance saturation from masking RL gains, we train on pruned subsets of the total 1,692 trajectories: π_0 uses 58 trajectories for Spatial/Object/Goal and 208 for Long; $\pi_{0.5}$ uses a unified

Table 1. Success rates (%) on LIBERO in the few-shot setting.

Model	Spatial	Object	Goal	Long	Avg.	Δ Avg.	
# Full SFT							
Octo (Ghosh et al., 2024)	78.9	85.7	84.6	51.1	75.1	—	
OpenVLA (Kim et al., 2024)	84.7	88.4	79.2	53.7	76.5	—	
π_{full} (Pertsch et al., 2025)	96.4	96.8	88.6	60.2	85.5	—	
OpenVLA-OFT (Kim et al., 2025b)	91.6	95.3	90.6	86.5	91.0	—	
π_0	96.8	98.8	95.8	85.2	94.2	—	
$\pi_{0.5}$	98.8	98.2	98.0	92.4	96.9	—	
# Few-shot SFT + RL							
SFT	65.3	64.4	49.8	51.2	57.6	—	
π_0	π_{RL} (Flow-SDE + PPO)	98.4	99.4	96.2	90.2	96.0	+38.4
	π_{RL} (Flow-SDE + GRPO)	97.8	97.8	83.2	81.4	90.0	+32.4
	π -StepNFT	93.5	98.0	83.7	86.7	90.5	+32.9
# Few-shot SFT + RL							
SFT	84.6	95.4	84.6	43.9	77.1	—	
$\pi_{0.5}$	π_{RL} (Flow-SDE + PPO)	99.6	100	98.8	93.0	97.9	+20.8
	π_{RL} (Flow-SDE + GRPO)	97.4	99.8	91.2	77.6	91.5	+14.4
	π -StepNFT	97.8	100	98.2	79.8	94.0	+16.9

Table 2. Success rates (%) on ManiSkill across In-Distribution (IND) and Out-Of-Distribution (OOD) settings.

Model	IND	OOD				
		Vision	Semantic	Execution	Avg.	
π_0	Full SFT	38.4	32.6	8.4	13.2	18.1
	π_{RL} (Flow-SDE + PPO)	78.8	61.1	25.4	31.5	39.3
	π -StepNFT	79.2	69.1	49.1	33.1	50.4
$\pi_{0.5}$	Full SFT	40.1	40.2	16.6	22.4	26.4
	π_{RL} (Flow-SDE + PPO)	90.9	68.0	34.5	45.4	49.3
	π -StepNFT	85.4	76.9	56.6	45.1	59.5

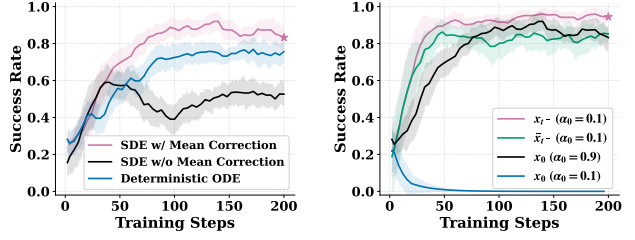
few-shot set of 40 trajectories (1 per sub-task). As for ManiSkill, we use the full 16,384 trajectories due to task complexity.

RL Training Protocol. We freeze the VLM backbone and fine-tune only the action expert. Training utilizes the RLinf (Yu et al., 2025) framework, which maximizes throughput by co-locating the environment, rollout policy, and actor on the same GPU. Main experiments were conducted on $8 \times$ NVIDIA H100 (80GB) GPUs; ablations used $8 \times$ NVIDIA RTX 4090 (48GB). Hyperparameters are detailed in the Appendix C.2.

5.2. Main Results

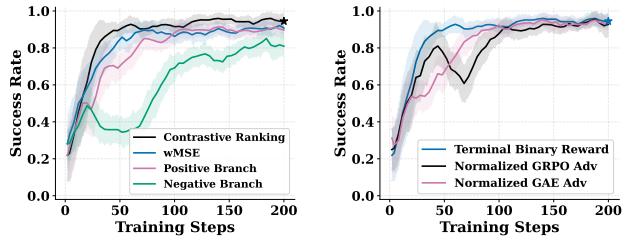
LIBERO: Unlocking potential from few-shot SFT.

Table 1 reveals that SFT baselines are constrained by a narrow expert manifold, yielding initial success rates of only 57.6% (π_0) and 77.1% ($\pi_{0.5}$). π -StepNFT unlocks the model’s latent capacity via “wider space” exploration, significantly boosting average performance to 90.5% and 94.0%, respectively. Notably, on short-horizon tasks (e.g., Object), our method achieves performance comparable to PPO. Regarding alignment, while critic-based methods (PPO) maintain an advantage in long-horizon tasks due to temporal credit assignment, our method notably outperforms the critic-free GRPO baseline (e.g., 86.7% vs. 81.4% on π_0 Long), demonstrating that step-wise supervision offers



(a) Stochastic rollouts. ODE vs. vs. Flow-SDE variants. (b) Regression target. x_0 vs. step-wise x_{t-} supervision.

Figure 2. Flow-SDE sampling and step-wise supervision improve on-policy stability.



(a) Loss formulation. wMSE vs. contrastive ranking. (b) Critic-free learning. Sparse labels vs. advantage signals.

Figure 3. Contrastive ranking enables stable critic-free learning.

highly competitive guidance without the need for estimating advantages.

ManiSkill: Critic-free generalization.

Unlike LIBERO, ManiSkill features high visual diversity, requiring generalization to unseen textures, objects and positions (OOD). Value-based methods estimate values from vision-language embeddings, which often causes critics to overfit to nuisance visual features and specific language prompts rather than task semantics. π -StepNFT bypasses this by relying on ground-truth outcomes. As shown in Table 2, while PPO is competitive in IND settings, π -StepNFT dominates in OOD scenarios. For π_0 , it achieves an OOD average of 50.4% (+11.1% over PPO), nearly doubling success rates on Semantic shifts (unseen objects/instructions) to 49.1%. This robust trend holds for $\pi_{0.5}$ (59.5% OOD average vs. 49.3%), confirming that critic-free supervision effectively mitigates visual overfitting.

5.3. Ablations Studies

To verify the efficacy of π -StepNFT, we conduct a component-wise analysis aligned with the challenges identified in Section 1. First, we decouple the effects of *stochastic exploration*, investigating whether SDE sampling with noise-aware correction is strictly necessary for manifold expansion compared to deterministic ODEs. Second, we analyze *supervision granularity*, contrasting our step-wise

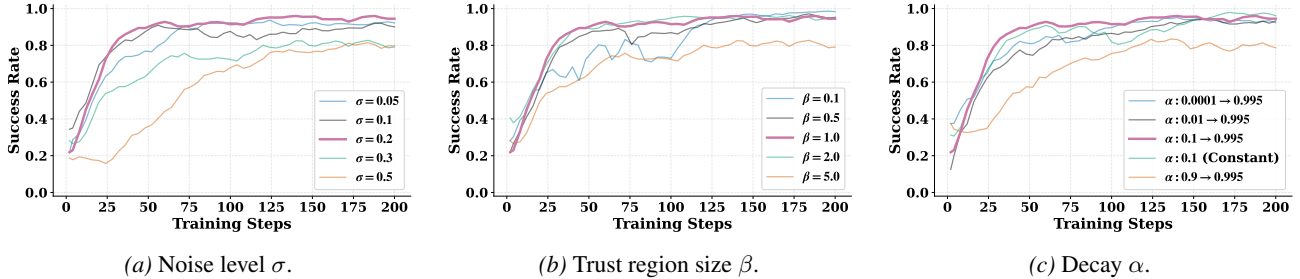


Figure 4. **Hyperparameter sensitivity analysis.** Configuration selected for main experiments is highlighted by the **bold pink** curves.

x_{t-} target against the standard terminal x_0 regression to demonstrate its impact on training stability and convergence speed. Third, we evaluate the *learning objective*, comparing our contrastive ranking formulation against weighted-MSE to highlight the benefits of removing the implicit separation penalty. Finally, we assess the necessity of *explicit critics*, showing that our likelihood-free framework achieves competitive performance using only sparse binary rewards, and provide a sensitivity analysis for key hyperparameters.

Impact of Stochastic Exploration. To isolate the benefit of exploration, we compare rollout strategies while fixing the regression target to the final denoised output x_0 and using a conservative EMA schedule ($\alpha: 0.9 \rightarrow 0.995$). As shown in Figure 2a, deterministic ODE rollouts ❶ (Figure 1) plateau early, confirming that restricted state coverage hinders policy improvement. While standard SDE ❷ widens the visited manifold, significant performance gains are only realized when the objective explicitly accounts for injected noise via mean correction ❸ (Eq. (3)). This indicates that effective exploration requires not just traversing a wider space, but utilizing a learning signal that mathematically aligns the noisy transition back to the policy’s velocity field.

Regression Target Granularity. We evaluate the efficacy of terminal x_0 versus step-wise x_{t-} regression targets under stochastic rollouts in Figure 2b. Empirical results demonstrate that supervision via x_0 induces significant instability, necessitating overly conservative synchronization to prevent policy collapse. Conversely, the step-wise target x_{t-} ❹ facilitates stable, near on-policy learning even under aggressive updates, thereby accelerating convergence. This suggests that precise, local supervision is essential to counteract the distribution shift introduced by active exploration, whereas terminal targets provide gradients that are too coarse for effective manifold adherence.

Objective Formulation: Ranking vs. wMSE. We benchmark the proposed contrastive ranking objective against a weighted-MSE (wMSE) baseline and single-branch ablations in Figure 3a. We observe that utilizing exclusively Positive or Negative branches yields partial improvement. This confirms that valid gradient signals exist in both directions, yet combining them yields superior performance.

Crucially, the wMSE baseline underperforms because, in the binary reward setting, it degenerates to fitting a single branch. Consequently, it fails to leverage both positive and negative signals simultaneously. In contrast, our ranking objective establishes a “push-pull” dynamic by utilizing both branches to enforce strict preference separation. This effectively removes the “implicit separation penalty” that otherwise suppresses the policy update magnitude.

Necessity of Value Estimation. We investigate the trade-off between supervision density and training complexity in Figure 3b. Although dense step-level value estimates can in principle improve long-horizon credit assignment, sparse trajectory-level outcomes remain highly competitive for general manipulation tasks. Empirically, binary supervision yields smoother training because it relies on accurate environment feedback rather than approximate value estimates. Unlike image generation, where sample quality varies continuously and advantage-style soft weighting is more natural, embodied control typically has discrete success-or-failure outcomes, similar to mathematical reasoning (Chen et al., 2026). Correspondingly, treating r as a bounded trajectory success probability $r \in [0, 1]$ avoids the instability of unbounded advantage scores and reduces the need for normalization and clipping. Our probability-based formulation is also compatible with denser supervision: the sparse signal can be replaced by an offline critic-learned that predicts step-wise success probabilities, enabling finer credit assignment without changing the architecture.

Hyperparameter Sensitivity and Robustness. Figure 4 illustrates key trade-offs. For noise level σ , excessive noise impedes convergence by overly expanding the search space, while insufficient noise limits exploration. For trust region size β , results indicate that values around [1.0, 2.0] are optimal; larger β violate local linearity, whereas smaller steps induce gradient instability. Regarding the decay α , a dynamic strategy proves most effective. High decay (slow updates) causes significant off-policy lag and lowers the performance ceiling, while constant or overly aggressive updates risk collapse. A dynamic schedule that progressively increases decay balances initial acceleration with final stability, which matches the small-step alignment in Theorem 4.4.

6. Conclusion

In this paper, we introduced π -StepNFT, a critic-and-likelihood-free framework for flow-based VLAs that structurally eliminates auxiliary value networks and requires only a single forward pass per step. We identified that wider exploration spaces necessitate finer-grained, step-wise guidance for effective alignment. Empirically, π -StepNFT unlocks latent potential on LIBERO in few-shot SFT settings and achieves superior OOD generalization on ManiSkill by preventing multimodal overfitting. These results establish a scalable, robust paradigm for fine-tuning generalist robot policies in complex real-world scenarios.

Impact Statement

This paper introduces a framework for fine-tuning flow-based vision-language-action (VLA) policies to improve the efficiency and robustness of embodied agents. Beyond algorithmic advances, our work has implications for the accessibility and sustainability of robotic learning.

Democratization of embodied AI research: Training large-scale VLA models often requires substantial compute, in part due to the cost of differentiating through ODE trajectories. By proposing a likelihood-free, critic-free approach that uses a single forward pass per optimization step, π -StepNFT lowers the hardware barrier. This reduced overhead can broaden participation by smaller labs and academic groups, supporting a more diverse research community.

Safety and robustness: By improving out-of-distribution (OOD) generalization, our method can yield agents that behave more reliably in unstructured real-world settings. While increased capability may introduce dual-use concerns, our fine-grained supervision encourages adherence to expert manifolds and may reduce unpredictable behaviors during deployment.

References

- Bai, J., Yu, X., Xu, M., Lu, W., Pan, X., Maeng, K., Kifer, D., Wang, J., and Wang, Y. Towards better optimization for listwise preference in diffusion models. *arXiv preprint arXiv:2510.01540*, 2025.
- Beyer, L., Steiner, A., Pinto, A. S., Kolesnikov, A., Wang, X., Salz, D., Neumann, M., Alabdulmohsin, I., Tschanen, M., Bugliarello, E., et al. Paligemma: A versatile 3b vlm for transfer. *arXiv preprint arXiv:2407.07726*, 2024.
- Bjorck, J., Castañeda, F., Cherniadev, N., Da, X., Ding, R., Fan, L., Fang, Y., Fox, D., Hu, F., Huang, S., et al. Gr00t n1: An open foundation model for generalist humanoid robots. *arXiv preprint arXiv:2503.14734*, 2025.
- Black, K., Janner, M., Du, Y., Kostrikov, I., and Levine, S. Training diffusion models with reinforcement learning. 2023.
- Black, K., Brown, N., Darpinian, J., Dhabalia, K., Driess, D., Esmail, A., Equi, M. R., Finn, C., Fusai, N., Galliker, M. Y., et al. $\pi_{0.5}$: a vision-language-action model with open-world generalization. In *9th Annual Conference on Robot Learning*, 2025.
- Black, K., Brown, N., Driess, D., Esmail, A., Equi, M., Finn, C., Fusai, N., Groom, L., Hausman, K., Ichter, B., Jakubczak, S., Jones, T., Ke, L., Levine, S., Li-Bell, A., Mothukuri, M., Nair, S., Pertsch, K., Shi, L. X., Tanner, J., Vuong, Q., Walling, A., Wang, H., and Zhilinsky, U. π_0 : A vision-language-action flow model for general robot control, 2026. URL <https://arxiv.org/abs/2410.24164>.
- Chen, H., Zheng, K., Zhang, Q., Cui, G., Cui, Y., Ye, H., Lin, T.-Y., Liu, M.-Y., Zhu, J., and Wang, H. NFT: Bridging supervised learning and reinforcement learning in math reasoning. In *The Fourteenth International Conference on Learning Representations*, 2026. URL <https://openreview.net/forum?id=ujBrsQm6Zu>.
- Chen, K., Liu, Z., Zhang, T., Guo, Z., Xu, S., Lin, H., Zang, H., Li, X., Zhang, Q., Yu, Z., Fan, G., Huang, T., Wang, Y., and Yu, C. π_{RL} : Online rl fine-tuning for flow-based vision-language-action models, 2025. URL <https://arxiv.org/abs/2510.25889>.
- Christiano, P. F., Leike, J., Brown, T., Martic, M., Legg, S., and Amodei, D. Deep reinforcement learning from human preferences. *Advances in neural information processing systems*, 30, 2017.
- Fan, J., Shen, S., Cheng, C., Chen, Y., Liang, C., and Liu, G. Online reward-weighted fine-tuning of flow matching with wasserstein regularization. In *The Thirteenth International Conference on Learning Representations*, 2025.
- Fan, Y., Watkins, O., Du, Y., Liu, H., Ryu, M., Boutilier, C., Abbeel, P., Ghavamzadeh, M., Lee, K., and Lee, K. Reinforcement learning for fine-tuning text-to-image diffusion models. In *Thirty-seventh Conference on Neural Information Processing Systems*, 2023. URL <https://openreview.net/forum?id=80TPepXzeh>.
- Ghosh, D., Walke, H., Pertsch, K., Black, K., Mees, O., Dasari, S., Hejna, J., Kreiman, T., Xu, C., Luo, J., Tan, Y. L., Chen, L. Y., Sanketi, P., Vuong, Q., Xiao, T., Sadigh, D., Finn, C., and Levine, S. Octo: An open-source generalist robot policy, 2024. URL <https://arxiv.org/abs/2405.12213>.

- Han, J., Wang, A., Xu, M., Chu, W., Dang, M., Yue, Y., and Ermon, S. Discrete diffusion trajectory alignment via stepwise decomposition. *arXiv preprint arXiv:2507.04832*, 2025.
- Ho, J., Jain, A., and Abbeel, P. Denoising diffusion probabilistic models. *Advances in neural information processing systems*, 33:6840–6851, 2020.
- Intelligence, P., Amin, A., Aniceto, R., Balakrishna, A., Black, K., Conley, K., Connors, G., Darpinian, J., Dhabalia, K., DiCarlo, J., et al. $\pi_{0.6}^*$: a vla that learns from experience. *arXiv preprint arXiv:2511.14759*, 2025.
- Kim, D., Lyu, S., Kim, S. W., and Seo, P. H. Direct diffusion score preference optimization via stepwise contrastive policy-pair supervision. *arXiv preprint arXiv:2512.23426*, 2025a.
- Kim, M. J., Pertsch, K., Karamcheti, S., Xiao, T., Balakrishna, A., Nair, S., Rafailov, R., Foster, E., Lam, G., Sankeeti, P., et al. Openvla: An open-source vision-language-action model. *arXiv preprint arXiv:2406.09246*, 2024.
- Kim, M. J., Finn, C., and Liang, P. Fine-tuning vision-language-action models: Optimizing speed and success. *arXiv preprint arXiv:2502.19645*, 2025b.
- Li, H., Zuo, Y., Yu, J., Zhang, Y., Yang, Z., Zhang, K., Zhu, X., Zhang, Y., Chen, T., Cui, G., et al. Simplevla-rl: Scaling vla training via reinforcement learning. *arXiv preprint arXiv:2509.09674*, 2025a.
- Li, Y., Ma, X., Xu, J., Cui, Y., Cui, Z., Han, Z., Huang, L., Kong, T., Liu, Y., Niu, H., et al. Gr-rl: Going dexterous and precise for long-horizon robotic manipulation. *arXiv preprint arXiv:2512.01801*, 2025b.
- Liao, X., Wei, W., Qu, X., and Cheng, Y. Step-level reward for free in rl-based t2i diffusion model fine-tuning. *arXiv preprint arXiv:2505.19196*, 2025.
- Lillicrap, T. P., Hunt, J. J., Pritzel, A., Heess, N., Erez, T., Tassa, Y., Silver, D., and Wierstra, D. Continuous control with deep reinforcement learning. *arXiv preprint arXiv:1509.02971*, 2015.
- Lipman, Y., Chen, R. T., Ben-Hamu, H., Nickel, M., and Le, M. Flow matching for generative modeling. *arXiv preprint arXiv:2210.02747*, 2022.
- Liu, B., Zhu, Y., Gao, C., Feng, Y., Liu, Q., Zhu, Y., and Stone, P. Libero: Benchmarking knowledge transfer for lifelong robot learning. *Advances in Neural Information Processing Systems*, 36:44776–44791, 2023.
- Liu, J., Liu, G., Liang, J., Li, Y., Liu, J., Wang, X., Wan, P., Zhang, D., and Ouyang, W. Flow-grpo: Training flow matching models via online rl. *arXiv preprint arXiv:2505.05470*, 2025.
- Liu, J., Gao, F., Wei, B., Chen, X., Liao, Q., Wu, Y., Yu, C., and Wang, Y. What can rl bring to vla generalization? an empirical study, 2026. URL <https://arxiv.org/abs/2505.19789>.
- Lu, G., Guo, W., Zhang, C., Zhou, Y., Jiang, H., Gao, Z., Tang, Y., and Wang, Z. Vla-rl: Towards masterful and general robotic manipulation with scalable reinforcement learning. *arXiv preprint arXiv:2505.18719*, 2025.
- McAllister, D., Ge, S., Yi, B., Kim, C. M., Weber, E., Choi, H., Feng, H., and Kanazawa, A. Flow matching policy gradients. *arXiv preprint arXiv:2507.21053*, 2025.
- Mu, T., Ling, Z., Xiang, F., Yang, D., Li, X., Tao, S., Huang, Z., Jia, Z., and Su, H. Maniskill: Generalizable manipulation skill benchmark with large-scale demonstrations. *arXiv preprint arXiv:2107.14483*, 2021.
- NVIDIA. Nvidia h100 tensor core gpu datasheet. Technical report, NVIDIA, 2022. URL <https://resources.nvidia.com/en-us-gpu-resources/h100-datasheet-24306>. Technical Report.
- NVIDIA. Nvidia ampere gpu architecture whitepaper. Technical report, NVIDIA, 2023. URL <https://images.nvidia.com/aem-dam/Solutions/geforce/ada/nvidia-ada-gpu-architecture.pdf>. Technical Report.
- Pan, C., Anantharaman, G., Huang, N.-C., Jin, C., Pfrommer, D., Yuan, C., Permenter, F., Qu, G., Boffi, N., Shi, G., et al. Much ado about noising: Dispelling the myths of generative robotic control. *arXiv preprint arXiv:2512.01809*, 2025.
- Pei, M., Li, G., Si, J., Zhu, Z., Mo, Z., Wang, P., Song, Z., Liang, X., and Cheng, J. Gcc: A 3dgs inference architecture with gaussian-wise and cross-stage conditional processing. In *Proceedings of the 58th IEEE/ACM International Symposium on Microarchitecture*, pp. 1824–1837, 2025.
- Pertsch, K., Stachowicz, K., Ichter, B., Driess, D., Nair, S., Vuong, Q., Mees, O., Finn, C., and Levine, S. Fast: Efficient action tokenization for vision-language-action models. *arXiv preprint arXiv:2501.09747*, 2025.
- Pfrommer, S., Huang, Y., and Sojoudi, S. Reinforcement learning for flow-matching policies. *arXiv preprint arXiv:2507.15073*, 2025.
- Rafailov, R., Sharma, A., Mitchell, E., Manning, C. D., Ermon, S., and Finn, C. Direct preference optimization: Your language model is secretly a reward model.

- Advances in neural information processing systems*, 36: 53728–53741, 2023.
- Schulman, J., Wolski, F., Dhariwal, P., Radford, A., and Klimov, O. Proximal policy optimization algorithms. *arXiv preprint arXiv:1707.06347*, 2017.
- Shukor, M., Aubakirova, D., Capuano, F., Kooijmans, P., Palma, S., Zouitine, A., Aractingi, M., Pascal, C., Russi, M., Marafioti, A., et al. Smolvla: A vision-language-action model for affordable and efficient robotics. *arXiv preprint arXiv:2506.01844*, 2025.
- Song, H., Qu, D., Yao, Y., Chen, Q., Lv, Q., Tang, Y., Shi, M., Ren, G., Yao, M., Zhao, B., et al. Hume: Introducing system-2 thinking in visual-language-action model. *arXiv preprint arXiv:2505.21432*, 2025.
- Song, Y., Sohl-Dickstein, J., Kingma, D. P., Kumar, A., Ermon, S., and Poole, B. Score-based generative modeling through stochastic differential equations. *arXiv preprint arXiv:2011.13456*, 2020.
- Steiner, A., Pinto, A. S., Tschannen, M., Keysers, D., Wang, X., Bitton, Y., Gritsenko, A., Minderer, M., Sherbondy, A., Long, S., et al. Paligemma 2: A family of versatile vlms for transfer. *arXiv preprint arXiv:2412.03555*, 2024.
- Sun, M., Ding, P., Zhang, W., and Wang, D. Iterative refinement of flow policies in probability space for online reinforcement learning. *arXiv preprint arXiv:2510.15388*, 2025.
- Sutton, R. S., McAllester, D., Singh, S., and Mansour, Y. Policy gradient methods for reinforcement learning with function approximation. *Advances in neural information processing systems*, 12, 1999.
- Wagenmaker, A., Nakamoto, M., Zhang, Y., Park, S., Yagoub, W., Nagabandi, A., Gupta, A., and Levine, S. Steering your diffusion policy with latent space reinforcement learning. *arXiv preprint arXiv:2506.15799*, 2025.
- Wallace, B., Dang, M., Rafailov, R., Zhou, L., Lou, A., Purushwalkam, S., Ermon, S., Xiong, C., Joty, S., and Naik, N. Diffusion model alignment using direct preference optimization. In *Proceedings of the IEEE/CVF Conference on Computer Vision and Pattern Recognition*, pp. 8228–8238, 2024.
- Wang, F. and Yu, Z. Coefficients-preserving sampling for reinforcement learning with flow matching. *arXiv preprint arXiv:2509.05952*, 2025.
- Williams, R. J. Simple statistical gradient-following algorithms for connectionist reinforcement learning. *Machine learning*, 8(3):229–256, 1992.
- Wu, Y.-L., Ruan, B.-K., Tseng, C., and Shuai, H.-H. Ranking-based preference optimization for diffusion models from implicit user feedback. In *The Thirty-ninth Annual Conference on Neural Information Processing Systems*, 2025.
- Yang, S., Zhang, Y., He, H., Pan, L., Li, X., Bai, C., and Li, X. Steering vision-language-action models as anti-exploration: A test-time scaling approach. *arXiv preprint arXiv:2512.02834*, 2025.
- Ye, A., Wang, B., Ni, C., Huang, G., Zhao, G., Li, H., Li, J., Zhu, J., Feng, L., et al. Gigabrain-0: A world model-powered vision-language-action model. *arXiv preprint arXiv:2510.19430*, 2025.
- Yu, C., Wang, Y., Guo, Z., Lin, H., Xu, S., Zang, H., Zhang, Q., Wu, Y., Zhu, C., Hu, J., et al. Rlinf: Flexible and efficient large-scale reinforcement learning via macro-to-micro flow transformation. *arXiv preprint arXiv:2509.15965*, 2025.
- Zhang, T., Da, C., Ding, K., Yang, H., Jin, K., Li, Y., Gao, T., Zhang, D., Xiang, S., and Pan, C. Diffusion model as a noise-aware latent reward model for step-level preference optimization. *arXiv preprint arXiv:2502.01051*, 2025a.
- Zhang, T., Yu, C., Su, S., and Wang, Y. Reinflo: Fine-tuning flow matching policy with online reinforcement learning, 2025b. URL <https://arxiv.org/abs/2505.22094>.
- Zheng, K., Chen, H., Ye, H., Wang, H., Zhang, Q., Jiang, K., Su, H., Ermon, S., Zhu, J., and Liu, M.-Y. DiffusionNFT: Online diffusion reinforcement with forward process. In *The Fourteenth International Conference on Learning Representations*, 2026. URL <https://openreview.net/forum?id=VJZ477R89F>.
- Ziegler, D. M., Stiennon, N., Wu, J., Brown, T. B., Radford, A., Amodei, D., Christiano, P., and Irving, G. Fine-tuning language models from human preferences. *arXiv preprint arXiv:1909.08593*, 2019.
- Zitkovich, B., Yu, T., Xu, S., Xu, P., Xiao, T., Xia, F., Wu, J., Wohlhart, P., Welker, S., Wahid, A., et al. Rt-2: Vision-language-action models transfer web knowledge to robotic control. In *Conference on Robot Learning*, pp. 2165–2183. PMLR, 2023.

A. Theoretical Analysis and Proofs

In this section, we provide detailed proofs for the lemmas, propositions, and theorems presented in the main text.

A.1. Proof of Equation 3 (Affine Mean Derivation)

We derive the explicit forms of U_t and B_t stated in Equation 3.

The flow-SDE solver computes the next mean $\mu_t(v)$ by mixing the rectified flow endpoints $x_0^{\text{pred}} = x_t - v \cdot t$ and $x_1^{\text{pred}} = x_t + v \cdot (1 - t)$ with weights derived from the Euler-Maruyama discretization. The weights are given by:

$$w_0 = 1 - t + \delta_t, \quad w_1 = (t - \delta_t) - \frac{\sigma_t^2 \delta_t}{2t}. \quad (14)$$

The mean is given by the linear combination:

$$\begin{aligned} \mu_t(v) &= w_0 x_0^{\text{pred}} + w_1 x_1^{\text{pred}} \\ &= w_0(x_t - vt) + w_1(x_t + v(1 - t)) \\ &= (w_0 + w_1)x_t + (-tw_0 + (1 - t)w_1)v. \end{aligned} \quad (15)$$

Directly computing the coefficients for x_t and v yields:

Coefficient for x_t (U_t):

$$U_t = w_0 + w_1 = (1 - t + \delta_t) + \left(t - \delta_t - \frac{\sigma_t^2 \delta_t}{2t}\right) = 1 - \frac{\sigma_t^2 \delta_t}{2t}. \quad (16)$$

Coefficient for v (B_t):

$$\begin{aligned} B_t &= -tw_0 + (1 - t)w_1 \\ &= -t(1 - t + \delta_t) + (1 - t) \left(t - \delta_t - \frac{\sigma_t^2 \delta_t}{2t}\right) \\ &= -t + t^2 - t\delta_t + (t - \delta_t) - \frac{\sigma_t^2 \delta_t}{2t} - t^2 + t\delta_t + t \frac{\sigma_t^2 \delta_t}{2t} \\ &= -\delta_t - (1 - t) \frac{\sigma_t^2 \delta_t}{2t}. \end{aligned} \quad (17)$$

Thus, $\mu_t(v) = U_t(x_t, t) + B_t(t)v$, matching the affine form in Equation (3). □

A.2. Proof of Lemma 4.2 (Log-Likelihood Ratio)

We prove that the difference in variance-normalized errors equals the log-likelihood ratio. Let $q(x) = \mathcal{N}(\mu, \Sigma)$. Its log-density is:

$$\log q(x) = -\frac{1}{2}(x - \mu)^\top \Sigma^{-1}(x - \mu) - \frac{1}{2} \log \det(2\pi\Sigma). \quad (18)$$

For the two branches $q_t^+ = \mathcal{N}(\mu_t^+, \Sigma_t)$ and $q_t^- = \mathcal{N}(\mu_t^-, \Sigma_t)$, they share the same covariance Σ_t . Subtracting their log-densities cancels the normalization constant:

$$\begin{aligned} \log q_t^+(x_{t-}) - \log q_t^-(x_{t-}) &= -\frac{1}{2} \left((x_{t-} - \mu_t^+)^\top \Sigma_t^{-1} (x_{t-} - \mu_t^+) - (x_{t-} - \mu_t^-)^\top \Sigma_t^{-1} (x_{t-} - \mu_t^-) \right) \\ &= -\frac{1}{2} \left(\|x_{t-} - \mu_t^+\|_{\Sigma_t^{-1}}^2 - \|x_{t-} - \mu_t^-\|_{\Sigma_t^{-1}}^2 \right) \\ &= -\frac{1}{2} (E_\theta^+ - E_\theta^-). \end{aligned} \quad (19)$$

This concludes the proof. □

A.3. Proof of Proposition 4.3 (Bayes Monotonicity)

Fix (x_t, c) and denote the prior success probability conditioned on (x_t, c) by $\pi(x_t, c) \triangleq \mathbb{P}(o = 1 \mid x_t, c) \in (0, 1)$.

By Bayes' rule, the posterior success probability given the observed next state x_{t-} is

$$\eta(x_{t-}; x_t, c) \triangleq \mathbb{P}(o = 1 \mid x_{t-}, x_t, c) = \frac{p(x_{t-} \mid x_t, c, o = 1) \pi(x_t, c)}{p(x_{t-} \mid x_t, c, o = 1) \pi(x_t, c) + p(x_{t-} \mid x_t, c, o = 0) (1 - \pi(x_t, c))}. \quad (20)$$

Define the oracle likelihood ratio

$$\Lambda(x_{t-}; x_t, c) \triangleq \frac{p(x_{t-} \mid x_t, c, o = 1)}{p(x_{t-} \mid x_t, c, o = 0)}.$$

Dividing the numerator and denominator by $p(x_{t-} \mid x_t, c, o = 0)$ yields

$$\eta(x_{t-}; x_t, c) = \frac{\Lambda(x_{t-}; x_t, c) \pi(x_t, c)}{\Lambda(x_{t-}; x_t, c) \pi(x_t, c) + (1 - \pi(x_t, c))}. \quad (21)$$

For constants $a = \pi(x_t, c) > 0$ and $b = 1 - \pi(x_t, c) > 0$, consider $f(\lambda) = \frac{a\lambda}{a\lambda + b}$ for $\lambda > 0$. Its derivative is

$$f'(\lambda) = \frac{ab}{(a\lambda + b)^2} > 0.$$

Therefore $\eta(x_{t-}; x_t, c)$ is strictly increasing in the likelihood ratio $\Lambda(x_{t-}; x_t, c)$, completing the proof. \square

A.4. Oracle Splits from Diffusion-NFT

Notation and symbol disambiguation. We use $\kappa_t(x_t \mid x_0)$ to denote the *forward/noising kernel* that maps a terminal sample x_0 to an intermediate noisy state x_t (as in diffusion models).

Setup. Fix a context c . Let x_0 denote the terminal sample (e.g., the final solver output used to form an action), with rollout terminal distribution $\pi_0^{\text{old}}(x_0 \mid c)$ induced by $\pi_{\theta^{\text{old}}}$. Let $\kappa_t(x_t \mid x_0)$ be the forward kernel and define the induced marginal

$$\pi_t^{\text{old}}(x_t \mid c) = \int \kappa_t(x_t \mid x_0) \pi_0^{\text{old}}(x_0 \mid c) dx_0,$$

and the diffusion posterior

$$\pi_{0|t}^{\text{old}}(x_0 \mid x_t, c) = \frac{\kappa_t(x_t \mid x_0) \pi_0^{\text{old}}(x_0 \mid c)}{\pi_t^{\text{old}}(x_t \mid c)}.$$

Optimality variable. Introduce a latent optimality variable $o \in \{0, 1\}$ and an instance-level score $r(x_0, c) \in [0, 1]$ satisfying $r(x_0, c) = \mathbb{P}(o = 1 \mid x_0, c)$. This is the same setup as Diffusion-NFT; see their Appendix for proofs.

Lemma A.1 (Distribution Split (Diffusion-NFT)). Let $p(c) \triangleq \mathbb{E}_{x_0 \sim \pi_0^{\text{old}}(\cdot \mid c)}[r(x_0, c)]$. Define the oracle terminal distributions

$$\pi_0^+(x_0 \mid c) = \frac{r(x_0, c) \pi_0^{\text{old}}(x_0 \mid c)}{p(c)}, \quad \pi_0^-(x_0 \mid c) = \frac{(1 - r(x_0, c)) \pi_0^{\text{old}}(x_0 \mid c)}{1 - p(c)}.$$

Then

$$\pi_0^{\text{old}}(x_0 \mid c) = p(c) \pi_0^+(x_0 \mid c) + (1 - p(c)) \pi_0^-(x_0 \mid c).$$

Reference. Diffusion-NFT Appendix (Distribution Split).

Lemma A.2 (Posterior Split (Diffusion-NFT)). Let $\pi_{0|t}^{\pm}(x_0 \mid x_t, c)$ be the posteriors induced by π_0^{\pm} :

$$\pi_{0|t}^{\pm}(x_0 \mid x_t, c) = \frac{\kappa_t(x_t \mid x_0) \pi_0^{\pm}(x_0 \mid c)}{\pi_t^{\pm}(x_t \mid c)}, \quad \pi_t^{\pm}(x_t \mid c) = \int \kappa_t(x_t \mid x_0) \pi_0^{\pm}(x_0 \mid c) dx_0.$$

Then the rollout posterior satisfies

$$\pi_{0|t}^{\text{old}}(x_0 \mid x_t, c) = \alpha(x_t, c) \pi_{0|t}^+(x_0 \mid x_t, c) + (1 - \alpha(x_t, c)) \pi_{0|t}^-(x_0 \mid x_t, c),$$

where the mixing weight is

$$\alpha(x_t, c) = \mathbb{P}(o = 1 \mid x_t, c) = p(c) \frac{\pi_t^+(x_t \mid c)}{\pi_t^{\text{old}}(x_t \mid c)}.$$

Reference. Diffusion-NFT Appendix (Posterior Split).

Corollary A.3 (Posterior Expectation Split). *Under Lemma A.2, for any integrable function $\phi(x_0)$,*

$$\mathbb{E}_{\pi_{0|t}^{\text{old}}(\cdot|x_t,c)}[\phi(x_0)] = \alpha(x_t,c) \mathbb{E}_{\pi_{0|t}^+(\cdot|x_t,c)}[\phi(x_0)] + (1 - \alpha(x_t,c)) \mathbb{E}_{\pi_{0|t}^-(\cdot|x_t,c)}[\phi(x_0)].$$

Oracle vs. constructed branches. The oracle objects $(\pi_0^\pm, \pi_{0|t}^\pm)$ are defined by conditioning on the latent outcome o . In contrast, our method constructs mirrored branches $v_\theta^\pm = v^{\text{old}} \pm \beta(v_\theta - v^{\text{old}})$ and the induced solver transitions $q_{\theta,t}^\pm(x_{t-} | x_t, c)$ (Section 4.1).

Lemma A.4 (Oracle Velocity/Mean Splits (for alignment)). *Assume the (oracle) velocity field at solver time t can be expressed as a posterior expectation under $\pi_{0|t}(\cdot | x_t, c)$, i.e., $v(x_t, c, t) = \mathbb{E}_{\pi_{0|t}(\cdot|x_t,c)}[\psi(x_0, x_t, c, t)]$ for some function ψ . Define oracle velocities v^\pm by taking the same expectation under $\pi_{0|t}^\pm$. Then*

$$v^{\text{old}}(x_t, c, t) = \alpha(x_t, c) v^+(x_t, c, t) + (1 - \alpha(x_t, c)) v^-(x_t, c, t).$$

If additionally the one-step solver mean admits the affine form $\mu_t(v) = A_t x_t + B_t v$ (Eq. 3), then

$$\mu_t^{\text{old}}(x_t, c) = \alpha(x_t, c) \mu_t^+(x_t, c) + (1 - \alpha(x_t, c)) \mu_t^-(x_t, c), \quad \Delta \mu_t^*(x_t, c) \triangleq \mu_t^+(x_t, c) - \mu_t^-(x_t, c) = B_t(v^+ - v^-).$$

Remark. This lemma is a direct consequence of Corollary A.3 and linearity of expectation.

A.5. Proof of Theorem 4.4 (Gradient Form and Alignment)

Fix a sampled training tuple (x_t, x_{t-}, c) collected under the rollout policy $v^{\text{old}} = \pi_{\theta^{\text{old}}}(c, x_t, t)$. Let the rollout one-step mean be $\mu_t^{\text{old}} := \mu_t(v^{\text{old}})$ and define the residual $e_t \triangleq x_{t-} - \mu_t^{\text{old}}$.

Recall that our constructed mirrored branches are $v_\theta^\pm = v^{\text{old}} \pm \beta(v_\theta - v^{\text{old}})$, $\Delta v_\theta \triangleq v_\theta - v^{\text{old}}$, and that the one-step mean admits the affine form (Eq. 3) $\mu_t(v) = A_t x_t + B_t v$, with shared covariance Σ_t .

Step 1: Constructed mean shift. Define the constructed branch means $\mu_{\theta,t}^\pm \triangleq \mu_t(v_\theta^\pm)$.

Using the affine mean form,

$$\mu_{\theta,t}^+ - \mu_t^{\text{old}} = B_t(v_\theta^+ - v^{\text{old}}) = B_t(\beta(v_\theta - v^{\text{old}})) = \beta B_t \Delta v_\theta \triangleq d_t, \quad (22)$$

$$\mu_{\theta,t}^{\text{old}} - \mu_{\theta,t}^- = B_t(v^{\text{old}} - v_\theta^-) = B_t(\beta(v_\theta - v^{\text{old}})) = d_t. \quad (23)$$

Hence,

$$\mu_{\theta,t}^\pm = \mu_t^{\text{old}} \pm d_t, \quad d_t = \beta B_t \Delta v_\theta. \quad (24)$$

Step 2: Error difference (Theorem 4.4.a). Recall the step errors $E_\theta^\pm = \|x_{t-} - \mu_{\theta,t}^\pm\|_{\Sigma_t^{-1}}^2$.

Substituting $\mu_{\theta,t}^\pm = \mu_t^{\text{old}} \pm d_t$ and $e_t = x_{t-} - \mu_t^{\text{old}}$ gives

$$\begin{aligned} E_\theta^+ - E_\theta^- &= \|e_t - d_t\|_{\Sigma_t^{-1}}^2 - \|e_t + d_t\|_{\Sigma_t^{-1}}^2 \\ &= (\|e_t\|_{\Sigma_t^{-1}}^2 + \|d_t\|_{\Sigma_t^{-1}}^2 - 2\langle e_t, d_t \rangle_{\Sigma_t^{-1}}) - (\|e_t\|_{\Sigma_t^{-1}}^2 + \|d_t\|_{\Sigma_t^{-1}}^2 + 2\langle e_t, d_t \rangle_{\Sigma_t^{-1}}) \\ &= -4\langle e_t, d_t \rangle_{\Sigma_t^{-1}} = -4\langle \Sigma_t^{-1} e_t, d_t \rangle, \end{aligned} \quad (25)$$

which proves part (a).

Step 3: Gradient form (Theorem 4.4.b). Define the logit $z_t \triangleq \frac{1}{2}y(E_\theta^+ - E_\theta^-)$, $\ell_t(\theta) = \text{softplus}(z_t)$.

Using $\nabla \text{softplus}(z) = \sigma(z)$,

$$\nabla_\theta \ell_t(\theta) = \sigma(z_t) \nabla_\theta z_t.$$

From Step 2,

$$E_\theta^+ - E_\theta^- = -4e_t^\top \Sigma_t^{-1} d_t,$$

thus

$$\nabla_{\theta} z_t = \frac{1}{2} y \nabla_{\theta} (E_{\theta}^{+} - E_{\theta}^{-}) = \frac{1}{2} y \nabla_{\theta} (-4e_t^{\top} \Sigma_t^{-1} d_t).$$

During optimization we treat the rollout branch v^{old} (hence μ_t^{old} and e_t) as constant with respect to θ , so only d_t depends on θ . From Equation (24), $d_t = \beta B_t (v_{\theta} - v^{\text{old}})$ and therefore

$$\nabla_{\theta} d_t = \beta B_t \nabla_{\theta} v_{\theta}, \quad \text{equivalently } (\nabla_{\theta} d_t)^{\top} = \left(\frac{\partial v_{\theta}}{\partial \theta} \right)^{\top} \beta B_t^{\top}.$$

Absorbing constant scalar factors into \propto , we obtain

$$-\nabla_{\theta} \ell_t(\theta) \propto \sigma(z_t) y \left(\frac{\partial v_{\theta}}{\partial \theta} \right)^{\top} B_t \Sigma_t^{-1} e_t, \quad (26)$$

which proves part (b).

Step 4: Small-step alignment (general $r \in [0, 1]$ and binary case). We relate the conditional expected update direction to an *oracle* improvement signal. Recall the signed label is defined in the main text as $y \triangleq 2r - 1$, $r \in [0, 1]$, where r is the observed terminal signal (e.g., success indicator or a normalized score).

Conditioned on (x_t, c) , the rollout residual $e_t \triangleq x_{t-} - \mu_t^{\text{old}}(x_t, c)$ is zero-mean since $\mu_t^{\text{old}}(x_t, c) = \mathbb{E}[x_{t-} \mid x_t, c]$, hence

$$\mathbb{E}[e_t \mid x_t, c] = 0. \quad (27)$$

Therefore,

$$\begin{aligned} \mathbb{E}[y e_t \mid x_t, c] &= \mathbb{E}[(2r - 1)e_t \mid x_t, c] \\ &= 2 \mathbb{E}[r e_t \mid x_t, c] - \mathbb{E}[e_t \mid x_t, c] \\ &= 2 \mathbb{E}[r e_t \mid x_t, c]. \end{aligned} \quad (28)$$

(i) *General case* ($r \in [0, 1]$). Equation (28) shows that the conditional expected direction is governed by the correlation between the terminal signal r and the local rollout residual e_t . In general, this produces a mixture of success- and failure-associated components (and does not reduce to a single oracle mean-gap direction without additional assumptions relating r to the latent optimality variable).

(ii) *Binary case* ($r \in \{0, 1\}$ with $r = o$). In sparse-success RL we often take r to be the episode success indicator, i.e., $r = o \in \{0, 1\}$ where o is the latent optimality variable. We have $\alpha(x_t, c) \triangleq \mathbb{P}(o = 1 \mid x_t, c)$ in Lemma A.2.

Then using the indicator property of o and Equation (27),

$$\begin{aligned} \mathbb{E}[y e_t \mid x_t, c] &= \mathbb{E}[(2o - 1)e_t \mid x_t, c] \\ &= 2 \mathbb{E}[o e_t \mid x_t, c] - \mathbb{E}[e_t \mid x_t, c] \\ &= 2 \mathbb{E}[o(x_{t-} - \mu_t^{\text{old}}) \mid x_t, c] \\ &= 2 \mathbb{P}(o = 1 \mid x_t, c) \mathbb{E}[x_{t-} - \mu_t^{\text{old}} \mid x_t, c, o = 1] \\ &= 2\alpha(x_t, c) (\mu_t^{+}(x_t, c) - \mu_t^{\text{old}}(x_t, c)), \end{aligned} \quad (29)$$

where $\mu_t^{+}(x_t, c) \triangleq \mathbb{E}[x_{t-} \mid x_t, c, o = 1]$ is the oracle success-branch mean.

By Lemma A.4, the oracle mean mixture identity holds:

$$\mu_t^{\text{old}}(x_t, c) = \alpha(x_t, c) \mu_t^{+}(x_t, c) + (1 - \alpha(x_t, c)) \mu_t^{-}(x_t, c),$$

hence

$$\mu_t^{+}(x_t, c) - \mu_t^{\text{old}}(x_t, c) = (1 - \alpha(x_t, c)) (\mu_t^{+}(x_t, c) - \mu_t^{-}(x_t, c)) = (1 - \alpha(x_t, c)) \Delta \mu_t^{*}(x_t, c),$$

where $\Delta \mu_t^{*}(x_t, c) \triangleq \mu_t^{+}(x_t, c) - \mu_t^{-}(x_t, c)$ is the oracle mean gap. Substituting into Equation (29) yields

$$\mathbb{E}[y e_t \mid x_t, c] = 2\alpha(x_t, c) (1 - \alpha(x_t, c)) \Delta \mu_t^{*}(x_t, c). \quad (30)$$

Finally, at the start of training (or for sufficiently small updates) where $v_\theta \approx v^{\text{old}}$ so that $\sigma(z_t) \approx \text{const}$, taking conditional expectation of the gradient form in Step 3 and using Equation (30) gives

$$\mathbb{E}[-\nabla_\theta \ell_t(\theta) \mid x_t, c] \parallel \left(\frac{\partial v_\theta}{\partial \theta} \right)^\top B_t \Sigma_t^{-1} \Delta \mu_t^*(x_t, c),$$

where scalar factors such as $2\alpha(1 - \alpha)$ do not affect alignment. This proves part (c). □

A.6. Proof of Theorem 4.5 (Comparison with wMSE)

A.6.1. DECOMPOSITION OF wMSE

We substitute $E_\theta^\pm = \|e_t \mp d_t\|_{\Sigma_t^{-1}}^2$ into the weighted-MSE objective $L_{\text{wMSE}} = rE_\theta^+ + (1 - r)E_\theta^-$. Expanding the terms immediately yields:

$$\begin{aligned} L_{\text{wMSE}} &= r(\|e_t\|^2 + \|d_t\|^2 - 2\langle \Sigma_t^{-1} e_t, d_t \rangle) + (1 - r)(\|e_t\|^2 + \|d_t\|^2 + 2\langle \Sigma_t^{-1} e_t, d_t \rangle) \\ &= (r + 1 - r)(\|e_t\|^2 + \|d_t\|^2) + 2\langle \Sigma_t^{-1} e_t, d_t \rangle(-r + (1 - r)) \\ &= \text{const} + \|d_t\|_{\Sigma_t^{-1}}^2 + 2(1 - 2r)\langle \Sigma_t^{-1} e_t, d_t \rangle. \end{aligned} \tag{31}$$

Using $y = 2r - 1$ (which implies $1 - 2r = -y$), we obtain:

$$L_{\text{wMSE}} = \text{const} - 2y\langle \Sigma_t^{-1} e_t, d_t \rangle + \|d_t\|_{\Sigma_t^{-1}}^2. \tag{32}$$

A.6.2. RANKING CALIBRATION

Define the ranking error event at a sampled step t :

$$\mathcal{E}_t := \{y(x_0, c) \cdot (E_\theta^+ - E_\theta^-) > 0\}. \tag{33}$$

π -StepNFT minimizes $\text{softplus}(y(E^+ - E^-))$, which is a convex upper bound on the indicator function $\mathbf{1}_{\mathcal{E}_t}$, thus directly minimizing ranking errors. In contrast, wMSE minimizes a regression loss with the penalty $\|d_t\|^2$ (from A.7.1), which restricts the branch separation required to satisfy the ranking condition \mathcal{E}_t when the margin is small.

A.6.3. BINARY CASE ANALYSIS

When $r \in \{0, 1\}$:

- **wMSE:** If $r = 1$, $L_{\text{wMSE}} = E^+$. It pulls μ^+ to x_{t-} but provides no signal to μ^- .
- **π -StepNFT:** Minimizes $\text{softplus}(E^+ - E^-)$. It simultaneously pulls μ^+ to x_{t-} and pushes μ^- away. This “push-pull” dynamic generates stronger gradients for discrimination. □

B. Detailed Related Works

B.1. Online RL for VLAs

VLA models map multimodal inputs to actions via diverse representations: discretizing actions into tokens (RT series (Zitkovich et al., 2023), OpenVLA (Kim et al., 2024)), mapping to continuous regression features (OpenVLA-OFT (Kim et al., 2025b)), or outputting actions via generative denoising processes (Octo (Ghosh et al., 2024), GR00T (Bjorck et al., 2025), OpenPi (Black et al., 2026; 2025; Intelligence et al., 2025)). While pre-training establishes broad capabilities, the post-training focus is shifting from SFT to online RL to bridge the domain gap. Adapting RL depends on these representations, where discrete approaches (VLA-RL (Lu et al., 2025), RL4VLA (Liu et al., 2026)) leverage accessible token probabilities, while continuous mappings (SimpleVLA-RL (Li et al., 2025a)) treat outputs as Gaussian means. However, flow-based VLAs face the challenge of intractable likelihoods due to multi-step ODE sampling. Some methods bypass likelihood calculation entirely: GR-RL (Li et al., 2025b) distills value functions in the latent space, while $\pi_{0.6}^*$ utilizes preference-based feedback. Conversely, π_{RL} (Chen et al., 2025) addresses this by transforming the deterministic ODE into an SDE or adding auxiliary noise networks. Crucially, this noise injection serves a dual purpose: it not only facilitates mathematical likelihood approximation but also significantly enhances exploration. This importance of noise-induced exploration is further echoed by test-time scaling strategies like TACO (Yang et al., 2025) and Hume (Song et al., 2025), as well as DSRL (Wagenmaker et al., 2025), which operates RL directly in the diffusion noise space.

B.2. Policy Optimization for Generative Models

Integrating online RL into generative models typically follows three paradigms to handle intractable likelihoods. Explicit Gradient and Advantage Methods. Approaches like DDPO (Black et al., 2023) and DPOK (Fan et al., 2023) treat denoising as a sequential decision process. Flow-GRPO (Liu et al., 2025) and ReinFlow (Zhang et al., 2025b) further facilitate this by converting ODEs to SDEs or using Gaussian approximations to enable policy gradient updates. Reward-Weighted Likelihood-Free Methods. To avoid exact likelihood computation, methods such as RWFm (Pfrommer et al., 2025; Fan et al., 2025) and FPO (McAllister et al., 2025) construct proxy objectives or advantage-weighted ratios, effectively optimizing the flow model via regression targets derived from high-reward samples. However, these paradigms often suffer from high variance in gradient estimation or rely on complex reward proxies to stabilize training. Preference and Contrastive Methods. These approaches align distributions via ranking losses, bypassing explicit advantages. Diffusion-DPO (Wallace et al., 2024) aligns models based on trajectory outcomes, while LPO (Zhang et al., 2025a) ensures fine-grained consistency at the latent noise-step level. Uniquely, Diffusion-NFT (Zheng et al., 2026) proposes a solver-agnostic framework that constructs implicit positive and negative update directions directly within the forward process, offering a computationally efficient paradigm without requiring explicit likelihoods or value networks.

C. Experiment Details

C.1. Detailed Introduction of Benchmarks

We evaluate on 2 multitask benchmarks.

- **LIBERO** (Liu et al., 2023): We follow the standard protocol across four suites (Spatial, Object, Goal, Long), reporting average success rates over 500 episodes (50 states \times 10 sub-tasks) per suite. The agent receives dual 224×224 RGB inputs, language instructions, and 7-dimensional proprioceptive states (6-DoF joints + gripper). It outputs continuous end-effector actions. The environment provides a sparse binary reward (1 for success, 0 otherwise).
- **ManiSkill** (Mu et al., 2021): We adopt the PutOnPlateInScene multitask setting from RL4VLA (Liu et al., 2026). This benchmark defines 4,352 compositional tasks derived from 16 objects, 17 receptacles, and 16 tabletop scenes. Observations consist of a single 480×640 third-person view, language instructions, and joint poses. Actions are continuous joint-space commands. The environment provides a composite reward to discourage degenerate throwing behaviors.

Table 3. OOD task mapping for ManiSkill PutOnPlateInScene25* across Vision, Semantics, and Execution categories.

Category	Sub-category (OOD type)	ManiSkill env IDs
Vision	Unseen Table (background)	PutOnPlateInScene25VisionImage-v1
	Dynamic Textures (foreground, weak)	PutOnPlateInScene25VisionTexture03-v1
	Dynamic Textures (foreground, strong)	PutOnPlateInScene25VisionTexture05-v1
	Dynamic Noise (image-level, weak)	PutOnPlateInScene25VisionWhole03-v1
	Dynamic Noise (image-level, strong)	PutOnPlateInScene25VisionWhole05-v1
Semantics	Unseen Objects	PutOnPlateInScene25Carrot-v1
	Unseen Receptacles	PutOnPlateInScene25Plate-v1
	Unseen Instruction Phrasings	PutOnPlateInScene25Instruct-v1
	Multi-Object	PutOnPlateInScene25MultiCarrot-v1
	Distractive Receptacle	PutOnPlateInScene25MultiPlate-v1
Execution	Unseen Position	PutOnPlateInScene25Position-v1
	Unseen Robot Init Pose	PutOnPlateInScene25EEPose-v1
	Mid-Episode Object Reposition	PutOnPlateInScene25PositionChangeTo-v1

C.2. Hyperparameters for Training

Table 4. Hyperparameter settings for Libero and ManiSkill.

Parameters	LIBERO								ManiSkill	
	π_0				$\pi_{0.5}$				π_0	$\pi_{0.5}$
	Spatial	Object	Goal	Long	Spatial	Object	Goal	Long	Multitask	Multitask
Train epochs	400	400	400	400	400	400	400	400	240	240
Batch size	2048	2048	2048	2048	2048	2048	2048	2048	5120	5120
Update epochs	2	2	4	4	1	1	3	4	5	5
Actor lr	1e-5	1e-5	1e-5	1e-5	1e-5	1e-5	1e-5	1e-5	8e-6	8e-6
Interaction steps	240	240	320	480	240	240	320	480	60	60
Parallel environments	64	64	64	64	64	64	64	64	64	64
Rollout epochs	8	8	8	8	8	8	8	8	–	–
Action chunk H	5	5	5	10	5	5	5	10	5	5
Denoise steps	4	4	4	4	4	4	4	4	4	4
Noise level σ	0.2	0.2	0.2	0.2	0.2	0.2	0.2	0.2	0.2	0.2
Trust Region Size β	1.0	1.0	1.0	1.0	1.0	1.0	1.0	1.0	1.0	1.0
Initial Decay α_0	0.1	0.1	0.1	0.1	0.1	0.1	0.1	0.1	0.1	0.1
End Decay α_{-1}	0.995	0.995	0.995	0.995	0.995	0.995	0.995	0.995	0.995	0.995

D. Additional Ablation: Step Selection Strategy

Motivation. Our step-wise supervision is defined on a single solver transition ($x_t \rightarrow x_{t-}$) sampled from a K -step Flow-SDE rollout. In our default implementation, we uniformly sample the solver step index $j \sim \mathcal{U}\{0, \dots, K-1\}$ at each training iteration and construct $(x_t, x_{t-}, t) = (x_{t_j}, x_{t_{j+1}}, t_j)$. This stochastic step selection exposes the model to transitions at different noise levels and denoising stages, providing more balanced supervision across the entire solver trajectory.

Ablation setup. We compare the default **Random Step** strategy against several **Fixed Step** variants, where the solver index j is held constant throughout training. All other configurations (solver, objective, training budget, and environment settings) remain identical.

Results. As shown in Figure 5, uniformly random step selection achieves more stable optimization and improves the final success rate compared to fixed-step choices. We hypothesize that fixed-step supervision biases learning toward a narrow noise regime, while random step selection provides coverage over multiple denoising stages and thus yields more robust policy learning.

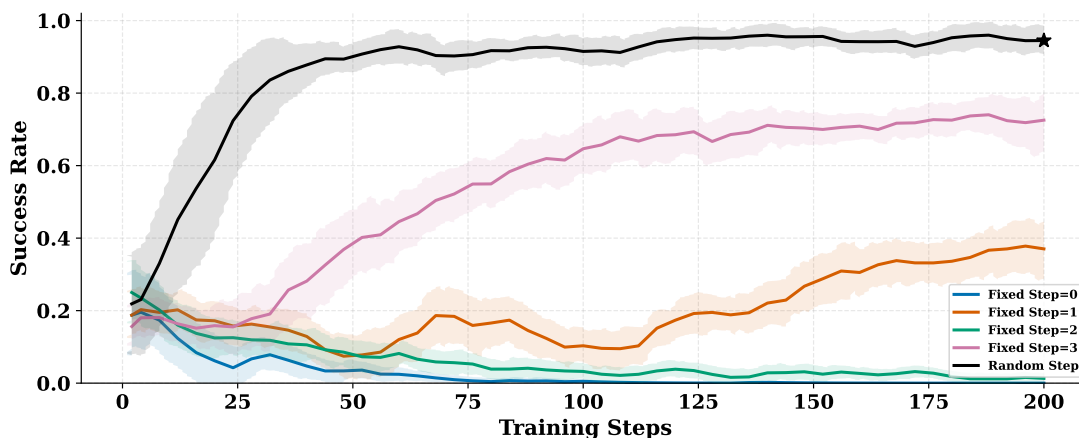


Figure 5. **Step selection ablation.** Performance comparison between uniform random solver-step sampling and fixed-step selection strategies.